Available online at www.sciencedirect.com

ScienceDirect

IFAC PapersOnLine 52-2 (2019) 102–107

A Scalable port-Hamiltonian Model for Incompressible Fluids in Irregular Geometries

Luis A. Mora * **Héctor Ramírez** * **Juan I. Yuz** *
Yann Le Gorrec **

* *Department of Electronic Engineering, Universidad Técnica Federico Santa María, Av. España 1680 Valparaíso, Chile (e-mail: luis.moraa@sansano.usm.cl, hector.ramireze@usm.cl, juan.yuz@usm.cl).*
** *FEMTO-ST, Univ. Bourgogne Franche-Comté, CNRS, 24 rue Savary, F-2500 Besançon, France (e-mail: yann.le.gorrec@ens2m.fr)*

Abstract: The behavior of a fluid in pipes with irregular geometries is studied. Departing from the partial differential equations that describe mass and momentum balances a scalable lumped-parameter model is proposed. To this end the framework of port-Hamiltonian systems is instrumental to derive a modular system which upon interconnection describes segments with different cross sections and dissipation effects. In order to perform the interconnection between different segments the incompressibility hypothesis is relaxed in some infinitesimal section to admit density variations and energy transference between segments. Numerical simulations are performed in order to illustrate the model.

© 2019, IFAC (International Federation of Automatic Control) Hosting by Elsevier Ltd. All rights reserved.

Keywords: Port-Hamiltonian systems, PDE, approximation of PDEs, computational methods

1. INTRODUCTION

A fluid is considered incompressible when its density is constant. In practice, to simplify the analysis of complex systems, it is common to consider as incompressible any fluid whose density variation is very small, i.e., that can be considered as negligible. The incompressibility approximation depends on the conditions to which the fluid is subjected . In an adiabatic process the flow of either a gas or a liquid can be considered incompressible when its Mach number, the ratio between the fluid and the sound velocities, is very small, i.e., the compressibility of a flow is associated with speed regimes. For Mach numbers less than 0.3 density variations are very small and the incompressible assumption is a very useful approximation (Johnson, 2016). This assumption for the airflow is usual in aerospace engineering (Wu and Cao, 2015), and bioengineering applications (Cal et al., 2017).

In areas such as waste water treatment (Hager, 2010) or arterial blood flow analysis (Guidoboni et al., 2009) the pipe presents geometric variations that produce changes in the flow velocities and energy losses associated with the pipe expansion and contraction. The fluid behavior in irregular geometries is commonly studied through distributed-parameters models. These models use numerical techniques, such as finite-volumes and LS-STAG, among others, that presents strong computational demands to obtain a detailed flow description (Bourantas et al., 2016; Sharatchandra and Rhode, 1994).

To reduce the complexity of fluid systems, a common engineering simplification is to consider the fluid as a one-dimensional flow described by a set of partial differential equations (PDEs). Additionally, to perform numerical computations the PDEs are approximated by sets of ordinary differential equations (ODEs). This allows to describe the fluid in different pipe sections.

On the other hand, the port-Hamiltonian (PH) framework is a useful mathematical tool to model systems (van der Schaft and Jeltsema, 2014). In a PH model the inputs and outputs are conjugated in the power sense, i.e., the product between inputs and outputs represents the supplied power. Additionally, dynamic of the system is characterized by a non-negative function that represents the total storage energy in the system and whose rate of change is bounded by the power supplied. A port-Hamiltonian model is focused in describe the energy flux in a system and provide of useful features as stability in Lyapunov sense, the state space norm is given by the system energy, the system is described through basic interconnectable energy storage elements, between others. These features provide nice properties such as passivity and scalability (van der Schaft, 2017; Duindam et al., 2009).

The behavior of fluids using infinite-dimensional port-Hamiltonian formulations has been studied in works as van der Schaft and Maschke (2002); Altmann and Schulze (2017). However to simulate these model it is necessary

⋆ This work was supported in part by CONICYT through grands CONICYT-PFCHA Bec. Doc. Nac. 2017-21170472, FONDECYT 1181090, MEC 80170066 and BASAL FB0008, also by the Agence Nationale de la Recherche- Deutsche Forschungs Gemeinschat (ANR-DFG) project INFIDHEM, ID ANR-16-CE92-0028 and the Agence Nationale de la Recherche project EIPHI-BFC ANR-17-EURE-0002

2405-8963 © 2019, IFAC (International Federation of Automatic Control) Hosting by Elsevier Ltd. All rights reserved.
Peer review under responsibility of International Federation of Automatic Control.
10.1016/j.ifacol.2019.08.018

to apply spatial discretization methods that preserve the PH structure, as they proposed in Kotyczka and Maschke (2017) and Trenchant et al. (2018). In an incompressible flow, under adiabatic conditions and neglecting the gravitational effects, the fluid only stores kinetic energy, i.e., the incompressibility hypothesis neglects the potential energy, due to the change of density, and hence makes the interconnection between sections non-causal.

In this paper we propose a scalable lumped port-Hamiltonian model to describe the behavior of incompressible fluids in irregular geometries. To this end we relax the incompressible hypothesis on some infinitesimal section to obtain a causal interconnection between different fluid sections.

This paper is organized as follows. In Section 2 we present the basics on PHS, the fluid behavior assumptions and develop the PHS model describing the fluid dynamic in a pipe with two sections. In Section 3 we extend the model to describe a pipe with n internal sections and dissipation associated with geometry variations in the pipes. In Section 4 we present two numerical examples to illustrate the behavior of the proposed model. Finally, in Section 5 we present the conclusion and discussions on future work.

2. A SIMPLE MODEL FOR THE INCOMPRESSIBLE FLUID

2.1 Port-Hamiltonian systems (PHS)

In this section we give a brief description on PHS. For a detailed overview see for instance van der Schaft and Jeltsema (2014). PHS are defined as follows

Definition 1. Consider $x \in \mathbb{R}^n$ as the vector of state variables and $H : \mathbb{R}^n \to \mathbb{R}$ as a scalar energy function, also called Hamiltonian. Consider $u \in \mathbb{R}^m$ and $y \in \mathbb{R}^m$ as the input and output respectively, such that y and u are conjugated in power sense. Thus, a PHS is given by following differential equation

$$\dot{x} = [J(x) - R(x)]\partial_x H + g(x)u \tag{1}$$

$$y = g(x)^T \partial_x H \tag{2}$$

where $J(x) = -J^T(x)$, $R(x) = R^T(x) \geq 0$ are $n \times n$ real matrices called interconnection and dissipation matrix respectively, and $g(x) \in \mathbb{R}^{n\times m}$ is the input matrix. The Hamiltonian H is a non-negative function whose rate of change is bounded as follow

$$\dot{H} \leq y^T u \tag{3}$$

where the product $y^T u$ represents the instantaneous power supplied to the system.

2.2 The fluid and the incompressibility assumption

The fluid dynamic is defined by a set of partial differential equations (PDEs) whose one-dimensional forms are given by

$$\partial_t \rho + \partial_z (\rho v) = 0 \tag{4}$$

$$\rho \partial_t v + \frac{\rho}{2}\partial_z v^2 + \partial_z p = 0 \tag{5}$$

where ρ and v are, respectively, the fluid density and velocity, and p is the static pressure. The PDEs in (4) and (5) represent the mass and momentum conservation laws for fluids, receptively (Bird et al., 2014).

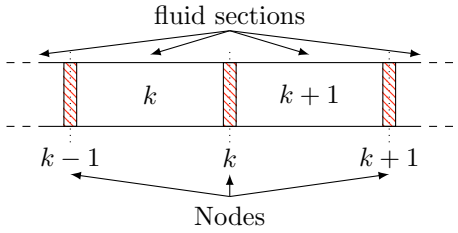

Fig. 1. Coupling incompressible fluid sections using a compressible behavior at the nodes

In a fluid the pressure is associated with the potential energy. Neglecting the gravitational effects and considering an isothermal fluid, the potential energy can be associated with the fluid work. However, under the incompressibility assumption the fluid work is zero and an instantaneous transmission of pressure from the boundary is assumed.

We shall assume that the variations of the fluid density are negligible, i.e., $\Delta\rho \lll \rho$. Thus, we consider that the flow in one section behaves as an incompressible fluid and that the compressibility effects occur in some infinitesimal volume, that shall be denoted by node and which is located in the coupling zone between two adjacent sections, as shown in Figure 1. To relax the incompressible hypothesis we consider the following assumption.

Assumption 1. During the expansion or contraction of a node the mass variations are much less than the volume variations. Hence, a uniform density distribution and a constant mass in each node is assumed, i.e., the following relationship is satisfied

$$\rho_j V_j = \kappa \tag{6}$$

where ρ_j and V_j are the density and volume in node j respectively, and κ is the corresponding node mass.

Then from this assumption, we develop a fluid model that allows a causal interconnection between adjacent fluid sections, as it's shown below.

2.3 Modeling a fluid section

The balance equation (5) represents the momentum conservation law without losses. However, when the pipe presents variations in its geometry, as contraction, expansion and changes in direction, it is known that energy losses occurs in the flow (Brodkey and Hershey, 2003). These losses are given by local turbulences that contribute significantly to the pressure drop. Thus, to include these effects and considering the incompressibility assumption, we rewrite the momentum balance as

$$\rho_0 \partial_t v = -\partial_z P - f_d(z) \tag{7}$$

where ρ_0 is the reference fluid density, $P = \frac{1}{2}\rho_0 v^2 + p$ is the total pressure field and $f_d(z)$ is a force associated with mechanical energy losses. Integrating (7) over the corresponding volume of section i, using the Leibnitz integral rule, the Gauss divergence theorem and considering an uniform cross-sectional area in the section, we obtain a finite-dimensional description of the fluid as follows,

$$\int \rho_0 \partial_t v dV_i = -\int \partial_z P dV_i - \int f_d(z) dV_i$$

$$\rho_0 V_i \dot{v}_i = A_i P_{1i} - A_i P_{2i} - A_i \int f_d(z) dz \quad (8)$$

where $\dot{v}_i$ is the time derivative of the average velocity in section i, A_i is the cross-sectional area, and P_{1i} and P_{2i} are the average pressures of the inlet and outlet boundary surfaces S_{1i} and S_{2i} respectively. According to Mulley (2004) the loss of mechanical energy in pipe contractions and expansions has been empirically associated with the dynamical pressure of the fluid. Thus, in a volume V_i we use the following approximation

$$\int f_d(z) dz \approx \lambda_i \frac{1}{2} \rho_0 v_i^2 \quad (9)$$

where the term $(\rho_0/2)\lambda_i v_i^2$ is the average pressure drop associated with the mechanical energy losses and λ_i is a dimensionless loss factor. Substituting (9) in (8), we can describe the dynamic behavior of the fluid in a section as

$$\rho_0 V_i \dot{v}_i = -A_i \frac{\rho_0}{2} \lambda_i v_i^2 + A_i P_{1i} - A_i P_{2i} \quad (10)$$

Defining $\pi_i = \rho_0 V_i v_i$ as the fluid momentum in section i and $K_i = \frac{1}{2} C_{xi} \pi_i^2$ as the corresponding kinetic energy, where $C_{xi} = 1/(\rho_0 V_i)$, the port-Hamiltonian formulation of (10) is given by

$$\dot{\pi}_i = -r_i \partial_{\pi_i} K_i + \begin{bmatrix} A_i & -A_i \end{bmatrix} \begin{bmatrix} P_{1i} \\ P_{2i} \end{bmatrix} \quad (11a)$$

$$\begin{bmatrix} Q_{1j} \\ -Q_{2j} \end{bmatrix} = \begin{bmatrix} A_i \\ -A_i \end{bmatrix} \partial_{\pi_i} K_i \quad (11b)$$

where $r_i = A_i \frac{\rho_0 \lambda_i \pi_i}{2 V_i}$ is term associated with the dissipation in section i, and Q_{1i} and Q_{2i} are the inlet and outlet volumetric flows. The definition of the dissipation factor λ_i depends on geometric changes in the pipe and will be discussed below.

2.4 The interconnection nodes

The model proposed in (11) represents the fluid behavior in an arbitrary section i. However, note that due to the causality of the model the input and output ports are not compatible for interconnection width adjacent sections. To solve this obstacle, we define an infinitesimal coupling zone between fluid sections, that shall be denoted as node. The conservation mass law in (4) is then rewritten as

$$\partial_t \rho_j = -\rho_j \partial_z v_j \quad (12)$$

Integrating (12) in the volume of node j and using the Gauss divergence theorem, the model that describe the fluid behavior in a node can be deduced as follow

$$\int \partial_t \rho_j dV_j = -\rho_j \int \partial_z v_j dV_j \quad (13a)$$

$$\dot{\rho_j} = \frac{\rho_j}{V_j} (Q_{1j} - Q_{2j}) \quad (13b)$$

where the Q_{1j} and Q_{2j} are the average flows in the inlet and outlet cross-sectional surfaces, S_{1j} and S_{2j}, of the corresponding node, respectively. Note that the inputs ports in (13b) are compatible with the outputs ports of adjacent fluid sections described by (11). To complete the coupling it is necessary to obtain an expression that relates the node pressure changes with the corresponding density variations. Then, using given the constant mass hypothesis of Assumption 1, we use the bulk modulus definition (Murdock, 1993), $\beta_S = -V_j(dp_j/dV_j)$, and (6) to write the differential of the pressure in a node as

$$dp_j = \frac{\beta_S}{\rho_j} d\rho_j \quad (14)$$

Considering that $p_j = 0$ when $\rho_j = \rho_0$ and solving (14), the pressure behavior in the j-th node is given by

$$p_j(\rho_j) = \beta_S \ln\left(\frac{\rho_j}{\rho_0}\right) \quad (15)$$

Considering a very small mass in a node, the kinetic energy can be neglected. Thus, the energy in an arbitrary node j, is given by the potential energy associated with the corresponding density variations. From the first law of thermodynamics and considering an adiabatic process, the potential energy in node j, E_j, is given by the fluid work, $dE_j = -p_j dV_j$. Using (6), the differential of the potential energy can be written as

$$dE_j = p_j \frac{\kappa}{\rho_j^2} d\rho_j \quad (16)$$

where p_j is the node pressure. From (16), the pressure in node j can be described as $p_j = (\rho_j^2/\kappa)\partial_{\rho_j} E_j$. The potential energy is then given by the following non-negative function

$$E_j(\rho_j) = \kappa \beta_S \frac{\rho_j - \rho_0 (1 + \ln(\rho_j/\rho_0))}{\rho_j \rho_0} \quad (17)$$

Finally, using (17) we can rewrite (13b) as the PHS

$$\dot{\rho_j} = 0 \partial_{\rho_j} E_j + \begin{bmatrix} \rho_j^2/\kappa & -\rho_j^2/\kappa \end{bmatrix} \begin{bmatrix} Q_{1j} \\ Q_{2j} \end{bmatrix} \quad (18a)$$

$$\begin{bmatrix} p_{1j} \\ -p_{2j} \end{bmatrix} = \begin{bmatrix} \rho_j^2/\kappa \\ -\rho_j^2/\kappa \end{bmatrix} \partial_{\rho_j} E_j \quad (18b)$$

2.5 The complete model

Consider a pipe composed in two sections, i.e., $i \in \{1, 2\}$ and $j = 1$. From (11), the sections are described by

$$\dot{\pi}_1 = -r_1 \partial_{\pi_1} K_1 + \begin{bmatrix} A_1 & -A_1 \end{bmatrix} \begin{bmatrix} P_{11} \\ P_{21} \end{bmatrix} \quad (19a)$$

$$\begin{bmatrix} Q_{11} \\ -Q_{21} \end{bmatrix} = \begin{bmatrix} A_1 \\ -A_1 \end{bmatrix} \partial_{\pi_i} K_1 \quad (19b)$$

$$\dot{\pi}_2 = -r_2 \partial_{\pi_2} K_2 + \begin{bmatrix} A_2 & -A_2 \end{bmatrix} \begin{bmatrix} P_{12} \\ P_{22} \end{bmatrix} \quad (20a)$$

$$\begin{bmatrix} Q_{12} \\ -Q_{22} \end{bmatrix} = \begin{bmatrix} A_2 \\ -A_2 \end{bmatrix} \partial_{\pi_2} K_2 \quad (20b)$$

where $K_1 = \frac{1}{2} C_{x1} \pi_1^2$ and $K_2 = \frac{1}{2} C_{x2} \pi_2^2$ are the kinetic energies in corresponding sections. On the other hand, from (18), the node is given by

$$\dot{\rho_1} = 0 \partial_{\rho_1} E_1 + \begin{bmatrix} \rho_1^2/\kappa & -\rho_1^2/\kappa \end{bmatrix} \begin{bmatrix} Q_{11} \\ Q_{21} \end{bmatrix} \quad (21a)$$

$$\begin{bmatrix} p_{11} \\ -p_{21} \end{bmatrix} = \begin{bmatrix} \rho_1^2/\kappa \\ -\rho_1^2/\kappa \end{bmatrix} \partial_{\rho_1} E_1 \quad (21b)$$

where E_1 is given by (17). Note that the input flows in (21) are compatible with the outputs Q_{21} in (19) and Q_{12} in (20). Similarly, the outputs in (21) are compatible width

the inputs P_{21} in (19) and P_{12} in (20). Thus, we obtain the following PHS

$$\begin{bmatrix}\dot{\pi}_1\\ \dot{\pi}_2\\ \dot{\rho}_1\end{bmatrix} = \begin{bmatrix} -r_1 & 0 & -A_1\frac{\rho_1^2}{\kappa}\\ 0 & -r_2 & A_2\frac{\rho_1^2}{\kappa}\\ A_1\frac{\rho_1^2}{\kappa} & -A_2\frac{\rho_1^2}{\kappa} & 0\end{bmatrix}\begin{bmatrix}\partial_{\pi_1}H\\ \partial_{\pi_2}H\\ \partial_{\rho_1}H\end{bmatrix} + \begin{bmatrix}A_1 & 0\\ 0 & -A_2\\ 0 & 0\end{bmatrix}\begin{bmatrix}P_{11}\\ P_{22}\end{bmatrix} \tag{22a}$$

$$\begin{bmatrix}Q_{11}\\ -Q_{22}\end{bmatrix} = \begin{bmatrix}A_1 & 0 & 0\\ 0 & -A_2 & 0\end{bmatrix}\begin{bmatrix}\partial_{\pi_1}H\\ \partial_{\pi_2}H\\ \partial_{\rho_1}H\end{bmatrix} \tag{22b}$$

where Q_{11} and Q_{22} are the inlet and outlet volumetric flows of the pipe, P_{11} and P_{22} the corresponding inlet and outlet pressures, and the total energy is given by

$$H = \kappa\beta_S\frac{\rho_1-\rho_0\left(1+\ln(\rho_1/\rho_0)\right)}{\rho_1\rho_0} + \sum_{i=1}^{2}\frac{1}{2}C_{xi}\pi_i^2 \tag{23}$$

3. A SCALABLE MODEL

The model proposed in (22) describes the behavior of two fluid sections. However, it is straightforward to extend the model to n fluid sections. First, for n fluid sections we define $\pi = [\pi_1, \pi_2, \cdots, \pi_n]^T$ as the momenta vector and $K = \sum_{i=1}^{n} K_i$ as the total kinetic energy, from (11) we describe the fluid behavior in n pipe sections as

$$\dot{\pi} = -R\partial_\pi K + [g_{\pi 1}\ -g_{\pi 2}]\begin{bmatrix}u_{\pi 1}\\ u_{\pi 2}\end{bmatrix} + g\begin{bmatrix}P_1\\ P_2\end{bmatrix} \tag{24a}$$

$$\begin{bmatrix}y_{\pi 1}\\ y_{\pi 2}\end{bmatrix} = \begin{bmatrix}g_{\pi 1}^T\\ -g_{\pi 2}^T\end{bmatrix}\partial_\pi K,\ \begin{bmatrix}Q_1\\ -Q_2\end{bmatrix} = g^T\partial_\pi K \tag{24b}$$

where P_1 and P_2 are the external pressures in the inlet and outlet boundary sections, respectively, Q_1 and Q_2 the corresponding volumetric flows, $u_{\pi 1} = [P_{12}, \cdots, P_{1n}]^T$ is the inlet pressure vector, $u_{\pi 2} = \left[P_{21}, \cdots, P_{2(n-1)}\right]^T$ is the outlet pressure vector, $y_{\pi 1} = [Q_{12}, \cdots, Q_{1n}]^T$ and $y_{\pi 2} = \left[Q_{21}, \cdots, Q_{2(n-1)}\right]^T$ are the internal inlet and outlet volumetric flow vectors, $R \in \mathbb{R}^{n\times n}$ is a dissipation matrix associated with energy losses due to geometry changes, and matrices $g \in \mathbb{R}^{n\times 2}$ and $\{g_{\pi 1}, g_{\pi 2}\} \in \mathbb{R}^{n\times(n-1)}$ are given by

$$g_{\pi 1} = \begin{bmatrix}0_{1\times(n-1)}\\ \text{diag}\left([A_2, \ldots, A_n]\right)\end{bmatrix}\quad g_{\pi 1} = \begin{bmatrix}\text{diag}\left([A_1, \ldots, A_{n-1}]\right)\\ 0_{1\times(n-1)}\end{bmatrix}$$

$$g = \begin{bmatrix}A_1 & 0\\ \mathbf{0} & \mathbf{0}\\ 0 & -A_n\end{bmatrix}$$

where $\mathbf{0}$ is a zero matrix of suitable dimensions. To obtain a description of the $n-1$ nodes we define $\rho = [\rho_1, \rho_2, \cdots, \rho_{n-1}]^T$ as the density vector and $E = \sum_{j=1}^{n-1} E_j$ as the fluid potential energy. Thus, from (18) the dynamic in the nodes is

$$\dot{\rho} = \mathbf{0}\partial_\rho E + [g_\rho\ -g_\rho]\begin{bmatrix}u_{\rho 1}\\ u_{\rho 2}\end{bmatrix} \tag{25a}$$

$$\begin{bmatrix}y_{\rho 1}\\ y_{\rho 2}\end{bmatrix} = \begin{bmatrix}g_\rho^T\\ -g_\rho^T\end{bmatrix}\partial_\rho E \tag{25b}$$

where $u_{\rho 1}$ is the inlet flow vector of the nodes, $u_{\rho 2}$ is the outlet flow vector, $y_{\rho 1}$ and $y_{\rho 2}$ are the inlet and outlet node pressures, respectively, and $g_\rho \in \mathbb{R}^{(n-1)\times(n-1)}$ is given by

$$g_\rho = \text{diag}\left(\left[\frac{\rho_1^2}{\kappa}, \ldots, \frac{\rho_{n-1}^2}{\kappa}\right]\right)$$

Notice that the input and output ports of (25) are compatible with the corresponding ports (24). Thus, for the interconnection of the fluid sections and the nodes we have

$$\begin{bmatrix}u_{\pi 1}\\ u_{\pi 2}\\ u_{\rho 1}\\ u_{\rho 2}\end{bmatrix} = \begin{bmatrix}\mathbf{0} & \mathbf{0} & \mathbf{0} & -I\\ \mathbf{0} & \mathbf{0} & I & \mathbf{0}\\ \mathbf{0} & -I & \mathbf{0} & \mathbf{0}\\ I & \mathbf{0} & \mathbf{0} & \mathbf{0}\end{bmatrix}\begin{bmatrix}y_{\pi 1}\\ y_{\pi 2}\\ y_{\rho 1}\\ y_{\rho 2}\end{bmatrix} \tag{26}$$

Finally, using (24), (25) and (26), the complete model is

$$\begin{bmatrix}\dot{\pi}\\ \dot{\rho}\end{bmatrix} = \begin{bmatrix}-R & J\\ -J^T & \mathbf{0}\end{bmatrix}\begin{bmatrix}\partial_\pi H\\ \partial_\rho H\end{bmatrix} + \begin{bmatrix}g\\ \mathbf{0}\end{bmatrix}\begin{bmatrix}P_1\\ P_2\end{bmatrix} \tag{27a}$$

$$\begin{bmatrix}Q_1\\ -Q_2\end{bmatrix} = \begin{bmatrix}g^T & \mathbf{0}\end{bmatrix}\begin{bmatrix}\partial_\pi H\\ \partial_\rho H\end{bmatrix} \tag{27b}$$

where P_1 and P_2 are the boundary pressures of pipe, Q_1 and Q_2 are the corresponding inlet and outlet volumetric flows, $J = (g_{\pi 1} - g_{\pi 2})\, g_\rho^T$ and the total energy is given by

$$H = \sum_{i=1}^{n}\frac{1}{2}\frac{\pi_i^2}{\rho_0 V_i} + \sum_{j=1}^{n-1}\kappa\beta_S\frac{\rho_j-\rho_0\left(1+\ln(\rho_j/\rho_0)\right)}{\rho_j\rho_0} \tag{28}$$

The definition of the loss factor λ_i depends on the geometry variation of the pipe and the class of bifurcation junctions (Mulley, 2004; Pérez-García et al., 2010). In this work we shall only consider the loss factors associated with sudden expansions and contractions. In a sudden expansion, when the fluid enters a section with enlarged cross-sectional area, a jet is formed as the fluid separates from the wall of the smaller pipe section. This jet expands until it fills the entire area and some fluid break away and circulates in the corner of the expanded section (Mulley, 2004). In this case the loss factor is given by

$$\lambda_i^e = \left(1 - \frac{A_i}{A_{i+1}}\right)^2 \tag{29}$$

In a sudden contraction given the reduction of the pipe, the fluid accelerates as it enters the smaller section. The loss factor is given by (Mulley, 2004)

$$\lambda_i^c = \frac{1}{2}\left(1 - \frac{A_i}{A_{i-1}}\right) \tag{30}$$

According to Brodkey and Hershey (2003), the loss factor in the inlet depends of the entrance pipe geometry and is usually less than 0.78, while the loss factor associated with the outlet is equal to 1. From these considerations the dissipation matrix in (27) is

$$R = \text{diag}\left(\left[A_1\frac{\rho_0\lambda_1\pi_1}{2V_1}, \ldots, A_n\frac{\rho_0\pi_n}{2V_n}\right]\right)$$

where each $\lambda_i, i \in [1, n-1]$ are define by λ_i^e or λ_i^c depending of the internal geometry and the loss factor in the last section is $\lambda_n = 1$.

4. NUMERICAL EXAMPLES

In this section we present two examples to illustrate the model. First a pipe with uniform cross sectional area with four fluid sections and uniform geometry is considered. Secondly a pipe with two cross sectional area changes,

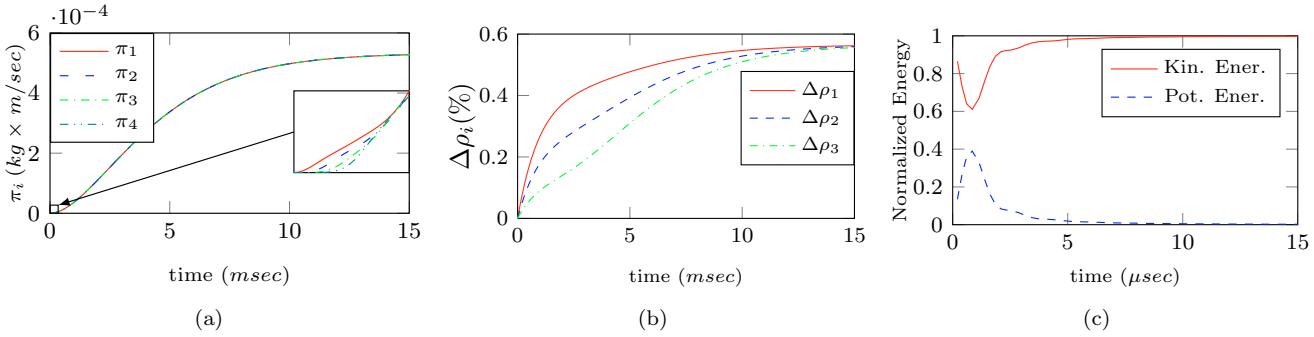

Fig. 2. Simulation results for example 1. (a) Momentum behavior in each fluid section, (b) Density variation in each node, (c) Normalized kinetic (red line) and potential (blue dashed line) energies

one contraction and one expansion, and six fluid sections is considered. The ODE15s solver of MATLAB is used in both examples. The fluid is air with density $\rho_0 = 1.1376 kg/m^3$ at $35°C$ and bulk modulus $\beta_S = 142 \times 10^3 Pa$. In practice a fluid is considered incompressible if the density variations are negligible. This implies that the potential energy of incompressible fluids is negligible in comparison with the corresponding kinetic energy. To evaluate that the model proposed in (27) satisfy these considerations, we analyze the density changes $\Delta\rho_i$ in each node using

$$\Delta\rho_i = 100\frac{\rho_j - \rho_0}{\rho_0} \tag{31}$$

and the normalized kinetic and potential energies in the system, $\bar{K}$ and $\bar{E}$, respectively, where

$$\bar{K} = \frac{\sum_{i=1}^{n} \frac{1}{2}\frac{\pi_i^2}{\rho_0 V_i}}{H} \tag{32}$$

$$\bar{E} = \frac{\sum_{j=1}^{n-1} \kappa\beta_S \frac{\rho_j - \rho_0\,(1+\ln(\rho_j/\rho_0))}{\rho_j\rho_0}}{H} \tag{33}$$

4.1 Example: A pipe with equal cross-sectional areas

Consider a pipe with transversal area A_0 and length L, divided in 4 sections with volume $V_0 = A_0 L/4$. The PHS (27) is given by

$$J = \frac{A_0}{k}\begin{bmatrix} -\rho_1^2 & 0 & 0 \\ \rho_1^2 & -\rho_2^2 & 0 \\ 0 & \rho_2^2 & -\rho_3^2 \\ 0 & 0 & \rho_3^2 \end{bmatrix} \qquad G = \begin{bmatrix} A_0 & 0 \\ 0 & 0 \\ 0 & 0 \\ 0 & -A_0 \end{bmatrix}$$

$$R = \text{diag}\left(\left[0, 0, 0, s_4 A_0 \frac{\rho_0 \pi_4}{2V_0}\right]\right)$$

Setting $A_0 = 5\times10^{-4}m^2$, $L = 0.1m$, $\kappa = 1\times10^{-10}kg$, $P_1 = 800Pa$ and $P_2 = 0Pa$, the simulation results are shown in Figure 2. Notice that the momentum presents a fast convergence to a uniform behavior in all sections (Figure 2.a). The density variation is less than 0.6% (Figure 2.b), i.e., for practical considerations it can be neglected. The energy is shown in Figure 2.c. Here the potential energy is significant only in the first microseconds of the simulation, being the kinetic energy is dominant. All these results are in concordance with the conditions used traditionally to assume the incompressible hypothesis (Johnson, 2016).

4.2 Example. A pipe with different cross sectional areas

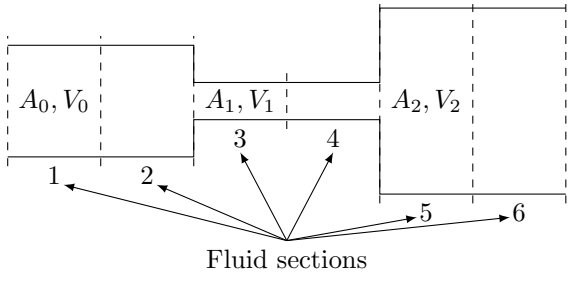

Fig. 3. Pipe with irregular geometry

Consider a pipe with sections that contracts and expands, as shown in Figure 3. The PHS is given by

$$J = \frac{1}{k}\begin{bmatrix} -A_0\rho_1^2 & 0 & 0 & 0 & 0 \\ A_0\rho_1^2 & -A_0\rho_2^2 & 0 & 0 & 0 \\ 0 & A_1\rho_2^2 & -A_1\rho_3^2 & 0 & 0 \\ 0 & 0 & A_1\rho_3^2 & -A_1\rho_4^2 & 0 \\ 0 & 0 & 0 & A_2\rho_4^2 & -A_2\rho_5^2 \\ 0 & 0 & 0 & 0 & A_2\rho_5^2 \end{bmatrix}$$

$$G = \begin{bmatrix} A_0 & 0 & 0 & 0 & 0 & 0 \\ 0 & 0 & 0 & 0 & 0 & -A_2 \end{bmatrix}^T$$

$$R = \frac{\rho_0}{2}\text{diag}\left(\left[0, s_2 A_0 \frac{\lambda_2\pi_2}{V_0}, 0, s_4 A_1 \frac{\lambda_4\pi_4}{V_1}, 0, s_6 A_2 \frac{\pi_6}{V_2}\right]\right)$$

where $\lambda_2 = (1/2)(1 - A_1/A_0)$ and $\lambda_4 = (1 - A_1/A_2)^2$ are the loss factors associated with a sudden pipe contraction and expansion Hager (2010), respectively. Setting $A_0 = 5\times10^{-4}m^2$, $A_1 = 0.5A_0$, $A_2 = 2A_0$, $V_0 = 1\times10^{-5}m^3$, $V_1 = 0.5V_0$, $V_2 = 2V_0$, $\kappa = 1\times10^{-10}kg$, $P_1 = 800Pa$ and $P_2 = 0Pa$, we obtain the simulation shown in Figure 4. The air momentum and velocity in each section are shown in Figure 4.a and Figure 4.c, respectively. Notice that the momentum presents a fast convergence to the same value for all sections, and the velocities depend on the section area. Figure 4.b shows the density changes in the nodes. Notice that the density variation is less than 1 percent, similarly to the previous example. Figure 4.d shows the potential and kinetic energies.

5. CONCLUSION

In this paper, a simple scalable PHS model for incompressible fluids in irregular geometries has been proposed.

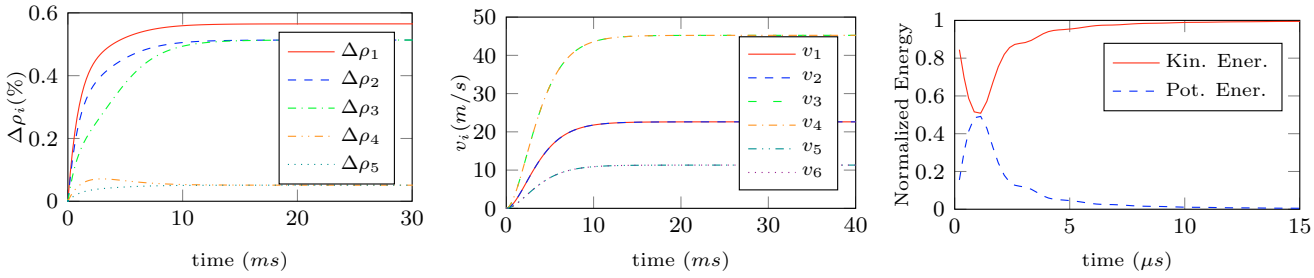

Fig. 4. Simulation results for example 2. (a) Density variation in each node, (b) Velocities behavior in each fluid section, (c) Normalized kinetic (red line) and potential (blue dashed line) energies.

Allowing small density variations in some infinitesimal pipe section we obtain a fluid description that allows the coupling of two adjacent incompressible fluid sections with a suitable energy transference. Two numerical examples have been carried out to show that the model preserve the features of incompressible fluids, density variations in coupling zones are very small, considered in practice as negligible, and the fluid potential energy is negligible compared with the kinetic energy. In future works, we consider to extend this method to pipes with time variable geometries, such as vocal folds and blood-vessels.

REFERENCES

Altmann, R. and Schulze, P. (2017). A port-Hamiltonian formulation of the Navier–Stokes equations for reactive flows. *Systems & Control Letters*, 100, 51–55.

Bird, R.B., Stewart, W.E., Lightfoot, E.N., and Klingenberg, D.J. (2014). *Introductory Transport Phenomena*. Jhon Wiley & Sons, United States of America.

Bourantas, G.C., Cheeseman, B.L., Ramaswamy, R., and Sbalzarini, I.F. (2016). Using DC PSE operator discretization in eulerian meshless collocation methods improves their robustness in complex geometries. *Computers & Fluids*, 136, 285–300.

Brodkey, R. and Hershey, H. (2003). *Transport Phenomena: A Unified Approach*. Chemical engineering series. Brodkey Publishing.

Cal, I.R., Cercos-Pita, J.L., and Duque, D. (2017). The incompressibility assumption in computational simulations of nasal airflow. *Computer Methods in Biomechanics and Biomedical Engineering*, 20(8), 853–868.

Duindam, V., Macchelli, A., Stramigioli, S., and Bruyninckx, H. (2009). *Modeling and Control of Complex Physical Systems*. Springer Berlin Heidelberg, Berlin, Heidelberg.

Guidoboni, G., Glowinski, R., Cavallini, N., Canic, S., and Lapin, S. (2009). A kinematically coupled time-splitting scheme for fluid–structure interaction in blood flow. *Applied Mathematics Letters*, 22(5), 684–688.

Hager, W.H. (2010). Losses in Flow. In *Wastewater Hydraulics*, 17–54. Springer Berlin Heidelberg, Berlin, Heidelberg, second edition.

Johnson, R. (2016). *The Handbook of Fluid Dynamics*. CRC Press, 2nd edition.

Kotyczka, P. and Maschke, B. (2017). Discrete port-Hamiltonian formulation and numerical approximation for systems of two conservation laws. *at - Automatisierungstechnik*, 65(5), 308–322.

Mulley, R. (2004). *Flow of Industrial Fluids: Theory and Equations*. CRC Press.

Murdock, J.W. (1993). *Fundamental Fluid Mechanics for the Practining Enegineer*, volume 82 of *Mechanical Engineering*. Marcel Dekker, Inc.

Pérez-García, J., Sanmiguel-Rojas, E., and Viedma, A. (2010). New coefficient to characterize energy losses in compressible flow at T-junctions. *Applied Mathematical Modelling*, 34(12), 4289–4305.

Sharatchandra, M.C. and Rhode, D.L. (1994). New, strongly conservative finite-volume formulation for fluid flows in irregular geometries using contravariant velocity components: Part 1. theory. *Numerical Heat Transfer, Part B: Fundamentals*, 26(1), 39–52.

Trenchant, V., Ramirez, H., Le Gorrec, Y., and Kotyczka, P. (2018). Finite differences on staggered grids preserving the port-Hamiltonian structure with application to an acoustic duct. *Journal of Computational Physics*, 373, 673–697.

van der Schaft, A.J. and Maschke, B.M. (2002). Hamiltonian formulation of distributed-parameter systems with boundary energy flow. *Journal of Geometry and Physics*, 42(1-2), 166–194.

van der Schaft, A. (2017). *L2-Gain and Passivity Techniques in Nonlinear Control*. Communications and Control Engineering. Springer International Publishing, Cham, 3rd edition.

van der Schaft, A. and Jeltsema, D. (2014). Port-Hamiltonian Systems Theory: An Introductory Overview. *Foundations and Trends® in Systems and Control*, 1(2-3), 173–378.

Wu, Z. and Cao, Y. (2015). Numerical simulation of flow over an airfoil in heavy rain via a two-way coupled Eulerian–Lagrangian approach. *International Journal of Multiphase Flow*, 69, 81–92.